Microscopic identification of the compensation mechanisms in Si-doped GaAs

C. Domke, Ph. Ebert, M. Heinrich, and K. Urban
Institut für Festkörperforschung, Forschungszentrum Jülich GmbH, 52425 Jülich, Germany
(Received 23 January 1996; revised manuscript received 16 May 1996)

The compensation mechanisms of Si_{Ga} donors in GaAs are determined by scanning tunneling microscopy. With increasing Si concentration the Si_{Ga} donors are consecutively electrically deactivated by Si_{As} acceptors, Si clusters, and Si_{Ga}-Ga-vacancy complexes. A microscopic model based on the screened Coulomb interaction between charged dopants, the amphoteric nature of Si, and the Fermi-level effect is proposed. It explains the observed defects, the critical Si concentrations of each identified mechanism, and predicts the solubility limit of Si in GaAs. [S0163-1829(96)02739-7]

The variation of the density and the chemical nature of dopant atoms provides the opportunity to engineer specific electronic properties of III-V compound semiconductors and to realize a wide field of electronic devices. Certain applications, e.g., diode lasers, require a high carrier concentration (greater than 1×10^{19} cm^{-3}), which is not always achievable, because of compensation effects. A technologically important example is the compensation of silicon (Si) donors in *n*-type GaAs. Si can be incorporated in GaAs on anion (arsenic, As) and cation (gallium, Ga) lattice sites as acceptor and donor, respectively. This amphotericity is known to reduce the doping efficiency of Si.[1] However, the autocompensation of Si_{Ga} donors by Si_{As} acceptors cannot solely explain the observed electrical deactivation of up to 99% of the Si donors.[2] Therefore, additional models for the compensation have been developed, such as the formation of Si pairs,[3] Si clusters,[4] and complexes of Si with a speculative native defect,[5,6] the existence of a nonhydrogenic Si level resonant with the conduction band,[7] and a variety of other mechanisms.

A direct experimental confirmation of the proposed models proved to be particularly difficult, because of the impossibility of obtaining an atomically resolved view inside of the crystal. Most experiments rely on the interpretation of vibrational-mode spectra or macroscopic crystal data and thus a reliable measurement of defect concentrations is difficult. Consequently, only limited conclusions on the atomic level were obtained.[6] In addition, diverse experiments and theories favor different compensation mechanisms.[6–8] Thus, the exact microscopic compensation mechanism of Si is still unclear and an atomically resolved real-space image of the existing point defects may be of great help for resolving the discrepancies.

In this paper, we demonstrate the direct identification of the compensation mechanisms of Si dopants in GaAs using atomically resolved scanning tunneling microscope (STM) images. We identify all defects occurring on (110) cleavage planes of Si-doped GaAs crystals and measure the concentrations per surface and/or subsurface layer of Si_{Ga} donors, Si_{As} acceptors, Si_n clusters, Ga vacancies (V_{Ga}), and Si_{Ga}-Ga-vacancy complexes (Si_{Ga}-V_{Ga}) separately. Using the measured concentrations per layer we calculate the *bulk* concentrations of each defect. We deduce the sequence and critical Si concentrations of the different consecutive compensation mechanisms and develop a microscopic model describing the activation of the successive compensation effects. A screened Coulomb interaction is found to govern the concentration of charged acceptors and donors as well as the solubility limit of Si in GaAs.

We investigated seed grown bulk GaAs crystals with three Si concentrations (c_{Si}): a low doped, vertical gradient freeze (VGF) grown crystal *A* with 55% of the Si compensated [carrier concentration (cc)$=1.2\times10^{18}$ cm^{-3} (measured using the Hall effect), c_{Si} [$=2.7\times10^{18}$ cm^{-3} measured by secondary-ion-mass spectroscopy (SIMS)]; a medium-doped, VGF grown sample *B* exhibiting a cc of 3.7×10^{18} cm^{-3} obtained with 1.3×10^{19} Si atoms cm^{-3} (72% compensation); and a highly doped, vertical Bridgeman grown sample *C* reaching a cc of only 1.2×10^{18} cm^{-3} at a Si density of $(2.5–6)\times10^{19}$ cm^{-3} (95% of the Si atoms do not contribute to the carrier concentration). The crystals were cleaved in UHV (5×10^{-9} Pa) and immediately transferred to the STM (in a dual-chamber system) without breaking the vacuum.[9]

STM images of the Si-doped GaAs (110) surfaces reveal a strong increase of the concentration of various defects with an increasing Si-doping concentration of the crystals. This suggests that the defects play a crucial role in the compensation. Therefore we analyze simultaneously measured, high-resolution STM images of the occupied (Fig. 1 panels a1–e1) and empty states (Fig. 1 panels a2 to e2) of all defects to identify them and evaluate their concentrations. In the following, we will address each defect separately.

(i) *Gallium vacancy (V_{Ga}).* Frames (a1) and (a2) of Fig. 1 show the most common defect, which was identified previously to be a Ga surface vacancy.[10] One empty dangling bond [Fig. 2(a2)] is missing and the two neighboring occupied dangling bonds are raised (a1). The defect is surrounded by a reduced empty and increased occupied density of states. This indicates a local upward band bending due to a negative charge of the vacancy.[11]

(ii) *Si_{Ga} donor.* Frames (b1) and (b2) show a defect, which has been identified as the Si_{Ga} donor.[12] The defect is surrounded by an elevation in both images. This is due to a positive charge and has been explained by a tip-induced band bending modulating the charge-induced band bending.[12] The specific defect shown is a Si atom in the second subsurface layer on a Ga lattice site. We could distinguish Si_{Ga} in several subsurface layers by the alternating symmetry and decrease of the magnitude of elevation.[13–15]

(iii) *Si_{As} acceptors.* Frames (c1) and (c2) show a negatively charged defect (upward band bending). We observed

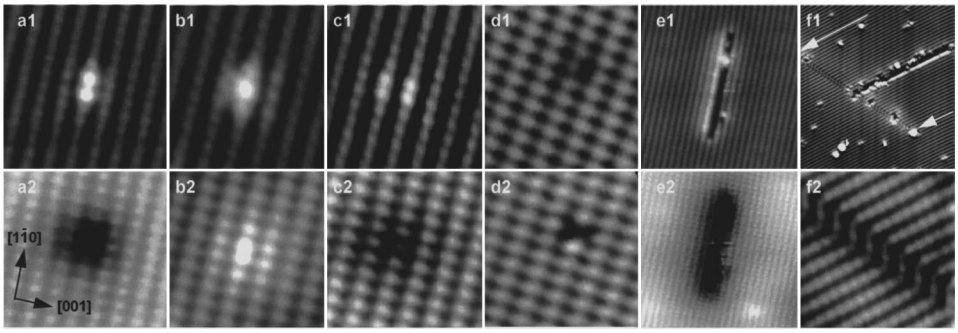

FIG. 1. Images of occupied (upper frames) and empty (lower frames) density of states of the major defects on Si-doped GaAs(110) surfaces (with the exception of frame f2). (a1) and (a2) show a Ga vacancy, (b1) and (b2) a Si_{Ga} donor, (c1) and (c2) a Si_{As} acceptor, (d1) and (d2) a Si_{Ga}-Ga-vacancy complex, (e1) and (e2) the intersection line of a planar Si cluster, and (f1) a dislocation close to a Si cluster (f2 is a zoom of the occupied states of the stacking fault in f1). The tunneling voltages are (a1) −2.4 V, (a2) +1.8 V, (b1) −2.0 V, (b2) +1.4 V, (c1) −2.0 V, (c2) +1.4 V, (d1) −2.0 V, (d2) +1.4 V, (e1) −2.2 V, (e2) +1.5 V, (f1) and (f2) −2.5 V. The defects were observed on cleavage planes of bulk crystals.

these defects in different subsurface layers. The symmetry analysis indicates that the defect is localized on an anion lattice site. The specific defect shown is in the second subsurface layer, as can be deduced from its symmetry. Compared to the Si donor it has a different symmetry due to its location on the other sublattice. The density of the defects increases with the Si concentration. The charge, the location, and the density point toward the Si_{As} acceptor. The presence of Si_{As} is expected due to the amphoteric nature of Si. Here we provide the first atomically resolved evidence for the Si_{As} acceptor.

(iv) *Dopant-vacancy complexes (Si_{Ga}-V_{Ga}).* In highly doped samples we observed an additional uncharged point defect [panels (d1) and (d2)]. The defect consists of a missing empty dangling bond (d2) and a slightly raised neighboring empty dangling bond. The concentration of the defect increases with increasing vacancy concentration and increasing Si concentration. This suggests that the defect consists of a combination of a vacancy and a Si atom. Close examination reveals a weak dipole character similar to Zn-dopant–anion-vacancy complexes.[15] Thus, we conclude that the defect in panels (d) is a (Si_{Ga}-V_{Ga}) complex. This is the first atomically resolved identification of the so-called Si-*X* complex.[5]

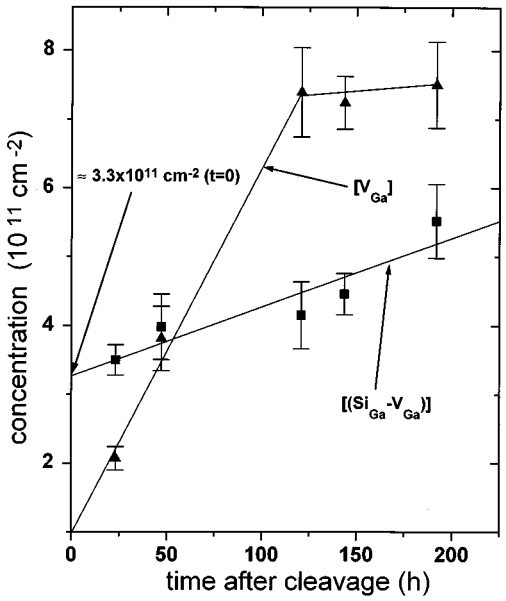

FIG. 2. Time dependence of the concentration of Ga vacancies and (Si_{Ga}-V_{Ga}) complexes. The vacancies are formed by Langmuir desorption and consequently the concentration of complexes increases with time too. The densities of the vacancies and complexes present directly after cleavage are estimated by extrapolation (solid line) to the cleavage time ($t=0$).

(v) *Si clusters.* With increasing Si concentration we observed a growing number of narrow trenches along the [110] direction. Their lengths ranged from 1 lattice spacing (corresponding to a Si pair) up to about 100 nm. We identify these trenches as Si clusters. Planar Si clusters on (111) planes were found in heavily Si-doped GaAs by transmission electron microscopy (TEM).[4] The [110] direction corresponds to the intersection line of such a (111) plane through a (110) surface. Close to some of the trenches we observed dislocations (frames *f*), in agreement with the TEM images. The geometric structure and the correlation with the Si density corroborate our identification of the trenches as planar Si clusters penetrating the surface. In addition, STM images reveal that the clusters disappear in samples annealed prior to cleavage above 1100 °C, in agreement with TEM measurements.[4]

At this stage we have to determine which defect is purely a surface defect and which is a bulk defect exposed on the surface by cleavage. The concentrations of most defects remain constant with time. However, Ga vacancies are formed thermally at room temperature on all *n*-type surfaces investigated, due to a low-temperature Langmuir desorption driven by the Fermi-level effect.[16] Thus, the Ga vacancies do not exist in the observed concentrations in the bulk. In order to deduce the bulk vacancy concentration, we monitored carefully the time dependence of the vacancy concentration (Fig. 2). By extrapolation to zero time after cleavage, we separate out vacancies formed after cleavage from those present in the bulk at the time of cleavage. With the assumption of no cleavage defects we calculate the bulk concentration. A similar procedure was followed for the dopant-vacancy complexes (Fig. 2), whose concentration is

TABLE I. Concentration of Si atoms per atomic layer incorporated into different defects (in 10^{10} cm^{-2}), as observed in the STM images. The concentration is given for the first and/or second subsurface layer for four Si containing defects. The concentration of the complexes is corrected for their increase after cleavage (see Fig. 2). Thus the values represent the concentration present in the crystal directly after cleavage (see text).

Defect	Subsurface layer	Sample A	Sample B	Sample C
Si_{Ga}^{+}	1st	5.4±1.1	4.9±2.3	5.6± 3.1
	2nd	1.3±0.6	3.1±1.7	3.3± 1.5
Si_{As}^{-}	1st	1.1±0.3	3.1±0.6	4.0± 0.4
	2nd	1.2±0.3	2.7±0.9	4.9± 1.2
Si_n cluster	1st	0.9±0.7	15.6±9.8	55 ±11
Si_{Ga}-V_{Ga}	1st	≈0	2.8±1.4	33 ± 5

connected with that of the vacancies. For sample *C* we obtained a complex density of $(3.3\pm0.5)\times10^{11}$ cm^{-2}.

In order to determine the *bulk* concentrations (of Si) from the *surface* concentrations (of Si containing defects) observable in the STM images, we have to evaluate for each type of defect the number of subsurface layers, in which the defect can be located and still be imaged by the STM. We distinguished the different subsurface positions of dopant atoms by the symmetry and intensity of the features observable in the STM images. The procedure that we followed has been demonstrated for a variety of dopant atoms[12,13,15] and for antisite defects[14] and we refer to the literature for further details. After the distinction of the different depth of the donors and acceptors, we measured the concentration of Si for each subsurface layer and each type of defect separately (Table I). From the data in Table I we can calculate the near surface (volume) concentrations, which reflect the bulk concentrations, if no diffusion occurred. Diffusion is indeed unlikely to occur at room temperature.

The measured *surface* concentrations for the Si acceptors and donors in the first and second subsurface layers is given in Table I separately. We found that the concentration per layer of the charged acceptors and donors remained constant with increasing depth, in agreement with previous measurements for a variety of dopant elements,[12,13,17] although the exact depth of Si_{Ga} in the third or deeper subsurface layers is more difficult to determine than for Si_{As}, because of the generally weaker signals. However, the counts of Si in the first two layers provided a reliable concentration value, which can be quite easily measured, because of the clear, unconfoundable appearance of high intensity in the STM images of Si acceptors and donors in the first and second subsurface layers. The clusters and the complexes could only be observed, if they where localized in the surface layer (the complexes are uncharged). Thus Table I gives the surface Si concentrations of those two defects. The Si concentration incorporated in the clusters per layer was determined by counting the number of lattice sites covered by the clusters.

The *bulk* concentrations of Si incorporated in the defects determined from the STM images are summarized in Fig. 3 as a function of the total Si dopant concentration incorporated into the crystals during growth. The latter has been measured by SIMS. The sum of the STM based Si concentrations in all defects agrees well with the expected total

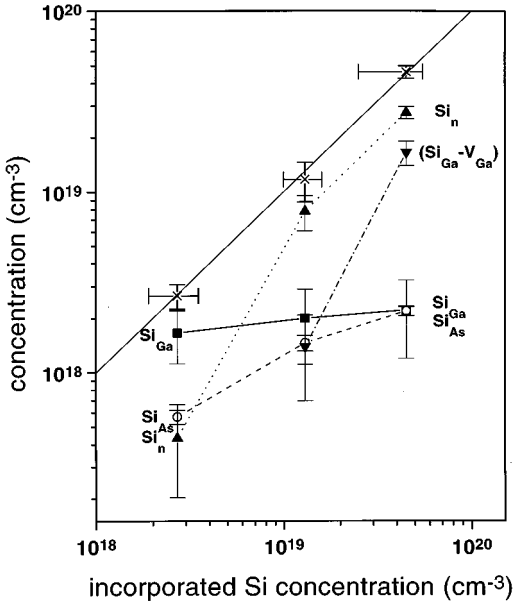

FIG. 3. Si concentration present in Si_{Ga} donors, Si_{As} acceptors, Si_n clusters, and (Si_{Ga}-V_{Ga}) complexes as a function of the Si-doping concentration incorporated into the crystals during growth. The Si-doping concentration incorporated during growth has been measured by secondary-ion-mass spectroscopy (SIMS). The sum of the Si concentrations of the different defects measured in the STM images (×) agrees well with that measured by SIMS (solid line). The horizontal error bars originate from the SIMS measurements. They should be applied to all the respective data points. All vertical error bars show the reproducibility of the STM measurements. The data is based on more than 3000 observations of Si atoms.

concentration of Si (measured by SIMS), indicating that we identified the Si containing defects correctly. The data reveals three trends: a nearly constant concentration of Si donors, a consecutive onset of three compensation mechanisms at specific critical Si concentrations, and the large majority of Si is not incorporated as donors.

The concentration Si_{As} is close to but always smaller than that of Si_{Ga} and the difference decreases with increasing Si doping. This agrees with theoretical predictions.[8,18] However, theory expects a strong increase of the concentration of donors and acceptors with the Si doping.[8] This is not observed here and the explanation, which we suggest, a screened-Coulomb-interaction limited solubility limit of Si in GaAs, will be addressed below.

At this stage we focus on the driving force of the consecutive onsets of the formation of first Si_{As} acceptors, second Si clusters, and finally (Si_{Ga}-V_{Ga}) complexes. Si is initially incorporated only on Ga sites as donors.[8] If Si would behave like an ideal donor, the carrier concentration would follow closely the density of Si and the screening of the charged Si dopants would become more and more efficient, resulting in no Coulomb repulsion between the Si donors up to Si concentrations in the range of $(0.5–1)\times10^{20}$ cm^{-3}.[19] A similar upper limit can be obtained by calculating the equilibrium between the screening length and the dopant concentration using Ref. 20. However, with increasing *n*-type doping the formation energy of Si_{As} acceptors decreases[18] and Si is increasingly incorporated on As sites as acceptors.[8] Thus the effective carrier concentration ($c(Si_{Ga})$-$c(Si_{As})$) is lower than

the Si concentration, reducing the efficiency of the screening and consequently Coulomb interactions become important. The situation can be modeled as a mixture of two gases with oppositely charged particles A and B in a fixed volume. The pressure of the gas is governed by the interaction between the particles, in this case the screened Coulomb interaction. At a certain concentration of particles, the pressure is high enough that the gas condensates, e.g., by forming uncharged (AB) particles. In analogy, the increasing number of positively charged Si_{Ga} donors and negatively charged Si_{As} acceptors interact and uncharged Si pairs are formed. The interaction starts as soon as the average distance of the Si atoms (8.1, 4.9, and 3.4 nm, in sample A, B, and C, respectively) becomes similar or smaller than the interaction range governed by the screening length. The latter is for the carrier concentrations present in our samples in the range of 4.2–6.3 nm at a temperature of 900 K.[20] In sample A the average distance is large enough to avoid most interaction effects and thus only few Si pairs are expected, in agreement with our observation. However, for the two stronger doped samples an interaction is likely to occur and Si pairs are formed. Those pairs may lead to larger Si clusters if Si-pair diffusion is possible, without any change of electrical properties. The formation of pairs and clusters leads to an increase of the average separation between the remaining charged Si donors and acceptors to values larger than the screening length (for sample A, B, and C: 8.9, 7.2, and 6.6 nm). This supports the view that the screened Coulomb interaction governs the solubility limit of Si in GaAs. Consequently, the density of charged Si donors and acceptors remains constant although the Si concentration increases by more than one order of magnitude, because the carrier concentration does not change much. This explains our observation of a nearly constant donor and acceptor concentration in contrast to theoretical predictions.

The above discussed compensation mechanism can never result in a decrease of the charge-carrier concentration with increasing Si-doping concentration, because Si is always incorporated preferentially as donor. At most a saturation is reached, if the Si atoms are equally incorporated on Ga and As sites. Thus, another mechanism must be responsible for the observed decrease of the charge-carrier concentration at high Si-doping concentrations.[2] The mechanism, which reduces the carrier concentration, is the formation of (Si_{Ga}-V_{Ga}) complexes. The Ga-vacancy formation energy is lowered with increasing n-type doping,[8,18] due to the *Fermi-level effect*.[21] Thus Ga vacancies are formed. The positively charged Si atoms attract the negatively charged vacancies[15] and vacancy-donor complexes are formed. The formation of complexes is an analogous mechanism to the one driving the Si pair formation. Both reduce the pressure of the Coulomb interactions.

In summary, we identified microscopically that Si_{As} acceptors, Si clusters, and Si_{Ga}-Ga-vacancy complexes compensate consecutively the Si dopants at specific critical Si concentrations. The observations are explained by a screened Coulomb interaction driving the Si-pair formation and thus governing the solubility limit of Si in GaAs. This successive formation of different defects explains the large amount of contradicting literature reporting different compensation mechanisms. Most of the proposed mechanisms contribute indeed, but dominate only in certain ranges of Si concentrations. Similar studies may help to understand doping difficulties in a variety of materials, such as p-type doping of ZnSe.[22] In addition, the present study demonstrates that interactions may alter considerably the theoretically expected concentrations of defects. Thus, the screened Coulomb interactions need to be taken into account for the theoretical modeling and understanding of charged defects and their concentrations in doped semiconductors.

The authors thank M. Althaus for providing the samples and K. H. Graf for technical support.

[1] J. M. Whelan, J. D. Struthers, and J. A. Ditzenberger, *Proceedings of the International Conference on Semiconductor Physics, Prague, 1960* (Publishing House of the Czechoslovac Academy of Sciences, Prague, 1961), p. 943.
[2] S. Schuppler *et al.*, Appl. Phys. Lett. **63**, 2357 (1993); Phys. Rev. B **51**, 10 527 (1995).
[3] C. Kolm, S. A. Kulin, and B. L. Averbach, Phys. Rev. **108**, 965 (1957).
[4] S. Muto *et al.*, Philos. Mag. A **66**, 257 (1992).
[5] J. Maguire *et al.*, Appl. Phys. Lett. **50**, 516 (1987).
[6] E. F. Schubert, *Doping in III–V Semiconductors* (University of Cambridge Press, Cambridge, 1993).
[7] T. N. Theiss, P. M. Mooney, and S. L. Wright, Phys. Rev. Lett. **60**, 361 (1988).
[8] J. E. Northrup and S. B. Zhang, Phys. Rev. B **47**, 6791 (1993).
[9] G. Cox *et al.*, Vacuum **41**, 591 (1990).
[10] G. Lengel, R. Wilkins, G. Brown, and M. Weimer, J. Vac. Sci. Technol. B **11**, 1472 (1993).
[11] J. A. Stroscio, R. M. Feenstra, and A. P. Fein, Phys. Rev. Lett. **58**, 1668 (1987); R. J. Hamers, J. Vac. Sci. Technol. B **6**, 1462 (1988).
[12] J. F. Zheng *et al.*, Phys. Rev. Lett. **72**, 1490 (1994).
[13] M. B. Johnson, O. Albrektsen, R. M. Feenstra, and H. W. M. Salemink, Appl. Phys. Lett. **63**, 2923 (1993); **64**, 1454(E) (1994).
[14] R. M. Feenstra, J. M. Woodall, and G. D. Pettit, Phys. Rev. Lett. **71**, 1176 (1993).
[15] Ph. Ebert *et al.*, Phys. Rev. B **53**, 4580 (1996).
[16] Ph. Ebert *et al.*, Phys. Rev. B **51**, 9696 (1995).
[17] J. F. Zheng, M. B. Salmeron, and E. R. Weber, Appl. Phys. Lett. **64**, 1836 (1994).
[18] R. W. Jansen and O. F. Sankey, Phys. Rev. B **39**, 3192 (1989).
[19] The upper concentration limit of dopant atoms, which can be incorporated without Coulomb interactions, can be deduced from M. B. Johnson *et al.*, Phys. Rev. Lett. **75**, 1606 (1995).
[20] R. B. Dingle, Philos. Mag. **46**, 831 (1955).
[21] T. Y. Tan, H.-M. You, and U. M. Gösele, Appl. Phys. A **56**, 249 (1993).
[22] A. Garcia and J. E. Northrup, Phys. Rev. Lett. **74**, 1131 (1995).